

## Article

# Preparation of Copper-Doped Zinc Oxide (CZO) Nanoparticles and CZO/Acrylic Copolymer Emulsion with Polyvinylpyrrolidone (PVP) Coated on Glass Substrate for Optical Properties

Pimpaka Putthithanas<sup>1</sup>, Sujittra Kaenphakdee<sup>1</sup>, Supan Yodyingyong<sup>2</sup> , Wannapong Triampo<sup>3</sup>, Noppakun Sanpo<sup>4</sup>, Jatorong Jitputti<sup>4</sup> and Darapond Triampo<sup>1,\*</sup> 

<sup>1</sup> Department of Chemistry and Center of Excellence for Innovation in Chemistry, Faculty of Science, Mahidol University, Phuttamonthon Sai 4 Road, Salaya, Nakhon Pathom 73170, Thailand; pimpaka.put@student.mahidol.ac.th (P.P.); sujittra.kae@student.mahidol.ac.th (S.K.)

<sup>2</sup> Institute for Innovative Learning, Mahidol University, Phuttamonthon Sai 4 Road, Salaya, Nakhon Pathom 73170, Thailand; supan.yod@mahidol.edu

<sup>3</sup> Department of Physics, Faculty of Science, Mahidol University, Phuttamonthon Sai 4 Road, Salaya, Nakhon Pathom 73170, Thailand; wannapong.tri@mahidol.ac.th

<sup>4</sup> SCG Chemical Co., Ltd., (SCG), 271 Sukhumvit Road, Muang District, Rayong 21150, Thailand; noppasnp@scg.com (N.S.); jjitputti@gmail.com (J.J.)

\* Correspondence: darapond.tri@mahidol.edu; Tel.: +66-87-915-1128

**Abstract:** This study investigated the effect of copper (Cu) doping content on zinc oxide with varied weight percentages and the dispersion of Cu-doped ZnO (CZO) by adding polyvinylpyrrolidone (PVP), coated on a glass substrate, through a physical assessment and optical property and thermal insulation testing. CZO NPs were synthesized by using the sol-gel method with a zinc acetate precursor. The powder X-ray diffraction (XRD) patterns of the CZO showed that the solid solubility limit was below 5 mol% without a secondary phase. A field-emission scanning electron microscopy (FE-SEM) micrograph demonstrated that the particle size of CZO was in nanoscale with the packing of a quasi-spherical shape. The UV-Vis-NIR reflectance spectra of the powder showed that 1 mol% CZO has the highest near-infrared (NIR) reflectivity in the wavelength 780–2500 nm, with great visible light transmission. The CZO NPs were loaded in acrylic copolymer in different weight percentages ranging from 25 wt% to 75 wt%, the film thickness of the coating was varied from 5  $\mu\text{m}$  to 100  $\mu\text{m}$ , and PVP was added into this nanocomposite polymer to disperse through an ultrasonication method. The results showed that the highest loading of CZO powder in a polymer at 75 wt% in 100  $\mu\text{m}$  of thickness with polyvinylpyrrolidone (PVP) as a dispersant showed better sample dispersion and retained good transparency to the naked eye.

**Keywords:** Cu-doped zinc oxide; coating; polyvinylpyrrolidone; optical property; dispersion; UV-Vis-NIR spectrophotometer



**Citation:** Putthithanas, P.; Kaenphakdee, S.; Yodyingyong, S.; Triampo, W.; Sanpo, N.; Jitputti, J.; Triampo, D. Preparation of Copper-Doped Zinc Oxide (CZO) Nanoparticles and CZO/Acrylic Copolymer Emulsion with Polyvinylpyrrolidone (PVP) Coated on Glass Substrate for Optical Properties. *Coatings* **2024**, *14*, 502. <https://doi.org/10.3390/coatings14040502>

Academic Editor: Chang Kwon Hwangbo

Received: 3 April 2024

Accepted: 15 April 2024

Published: 18 April 2024



**Copyright:** © 2024 by the authors. Licensee MDPI, Basel, Switzerland. This article is an open access article distributed under the terms and conditions of the Creative Commons Attribution (CC BY) license (<https://creativecommons.org/licenses/by/4.0/>).

## 1. Introduction

Zinc oxide (ZnO) is one of the most attractive oxide materials due to its unique properties and versatile applications in transparent electronic materials [1], ultraviolet (UV) light emitters [2,3], chemical sensors [4,5], solar cells [6], etc. ZnO is a direct band gap (3.36 eV at ambient temperature) n-type semiconductor and has a large exciton binding energy of 60 meV. It has high crystallinity, high thermal stability, high photoconductivity, good mechanical strength, and non-toxicity. ZnO with a hexagonal wurtzite structure in nanopowder has been prepared by various methods, which include solid-state reaction [7], the sonochemical method [8], the oxidation process [9], colloid chemistry [10], the hydrothermal method [11], the solution combustion method [12,13], the soft chemical

method [14], the organochemical route [15,16], the wet chemical method [17], the vapor condensation process [18], co-precipitation [19,20], the sol–gel method [21,22], and so on. Among these methods, the sol–gel process is of great interest for preparing the nanopowder because of its low equipment costs, simplicity, environmental safety, and ease of increasing the amount of powder. In order to improve the properties of ZnO, it is usually doped with group III elements such as Al, Ga, and In and the group VII elements Cl, I, and F, which act as substitutional elements for Zn and oxide, respectively. Among the various types of metal-doped ZnO, specifically, copper-doped ZnO (CZO) has attracted attention because of its low material costs, richness in the Earth's crust, and chemical stability. However, much less research work is being carried out on these CZO nanoparticles.

In this study, we were interested in using CZO nanoparticles with thermal insulating glass to shield against near-infrared (NIR) light and let visible light pass through the glass. One advantage of thermal insulating glass is that it blocks heat rays from sunlight that cause heat gain in buildings and automobiles with transparent glass. These properties can reduce interior air temperatures, keep inside areas cool, and reduce electricity usage, especially the use of electricity which would otherwise be used for air conditioning. Traditional glass lets most sunlight radiation transmit through the glass, making the inside temperature of the buildings and automobiles increase until they are uncomfortable to be in. For thermal insulating applications, recent work has involved the use of, for example,  $\text{Na}_x\text{WO}_3$ , which is synthesized via the solvothermal method, requiring a specific tool (autoclave), high temperature, and high pressure to synthesize and being difficult to scale-up [23]. Much research has been carried out on tungsten bronze ( $\text{M}_x\text{WO}_3$ ) as an NIR shielding material. W (tungsten) is an expensive metal and a rare earth. Our work has many advantages, as CZO nanoparticles are synthesized via the sol–gel method, which does not require specific equipment, is a low-cost synthesis technique, and is easy to scale-up. Cu and Zn are inexpensive and abundant in the Earth's crust, and much less research work has been carried out on CZO nanoparticles in thermal insulating glass applications.

CZO nanocomposite coatings have also attracted increasing interest in recent years, and the use of a dispersion coating is crucial to disperse CZO nanoparticles in the coating in a good way to ensure a smooth and uniform surface coating. Polyvinylpyrrolidone (PVP) is one of the most used dispersants in the coating process due to it being a strong capping agent, thus preventing the aggregation of nanoparticles via the steric effect that is based on its hydrophobic chains [24]. PVP is non-ionic, water-soluble in polymers and soluble in various solvents (e.g., water, alcohol, amide, and chlorinated solvents), non-toxic, and temperature-resistant. In this work, we added PVP to dispersed CZO nanoparticles in acrylic copolymer emulsion. However, the PVP concentration affects the structural and optical properties of the materials [25]. PVP is widely employed as a multifunctional material, being used as a binder due to its adhesive property, and it is used as a binder in many pharmaceutical tablets, such as those for drug delivery, etc.

For this reason, herein, we present our investigation of a synthesized ZnO that was doped with Cu metal via the sol–gel method due to its ease of preparation, its facilitation of the up-scaling of samples, and the fact that it is an environmentally friendly process. With Cu-doped zinc oxide (CZO) and acrylic copolymer emulsion as the model, CZO/acrylic copolymer composite coatings without/with PVP acted as dispersants and were prepared using the casting method. These coatings can transmit visible light (400–780 nm) and shield near-infrared (NIR) light (780–2500 nm). In high weight percentage loading of CZO powder to polymer, it presented a high transparency at 75 wt% CZO nanopowder. These coated glasses were investigated for their optical properties using a UV-vis-NIR spectrophotometer, and also, their thermal insulation was tested with an IR lamp irradiating the coated glass.

## 2. Materials and Methods

### 2.1. Materials

Zinc acetate ( $\text{Zn}(\text{CH}_3\text{COO})_2 \cdot 2\text{H}_2\text{O}$ , 99.0%), cupric acetate  $\text{Cu}(\text{CH}_3\text{COO})_2$ , and *mono*-ethanolamine (MEA) were purchased from Sigma Aldrich (St. Louis, MO, USA). Isopropanol

was procured from Fluka (Buchs, Switzerland). Ethanol (C<sub>2</sub>H<sub>5</sub>OH, 99.7%) was brought from Daejeon Chemicals Reagent (Daejeon, Republic of Korea). Acrylic copolymer emulsion was obtained from Thai Young Chemical (Bangkok, Thailand). Polyvinylpyrrolidone (PVP) M.W. 40,000 was secured from Alfa Aesar (Ward Hill, MA, USA). All the chemicals were used without any further purification for the fabrication of CZO.

## 2.2. Synthesis of CZO Powder

Cu-doped zinc oxide (CZO) NPs were synthesized by the sol–gel method. Zinc acetate was used as a precursor. First, 2 mL MEA was added to 50 mL isopropanol under stirring for a few minutes. Then, 0.3 M zinc acetate was added into the solution and stirred at 65 °C until a homogeneous solution was achieved. For the Cu solution, MEA was added in isopropanol, and then 0.3 M cupric acetate was added with the molar ratio of the dopant Cu/(Cu + Zn) at 0, 1, 5 and 10 mol%. The mix Zn solution and Cu solution were subjected to stirring at 65 °C for 1 h. The mix solutions were dried in an oven at 60 °C to remove the solvent, which was then calcinated in a furnace at 550 °C for 1 h. After that, it was ground with ceramic mortar into a fine CZO powder.

## 2.3. Preparation of CZO/Acrylic Copolymer Coating via Casting Technique

Microscope slides with a size of 1 inch × 1.5 inch and thickness of 1–1.2 mm were selected for coatings. The glass slides were immersed in HNO<sub>3</sub> and washed with soap solution and distilled water, and finally, the cleaned glass surface was dried in an oven at 60 °C.

For the preparation of a CZO/acrylic copolymer coating solution without PVP, 0 mol% and 1 mol% of CZO powder were ultrasonically dispersed in 25 mL of ethanol for a few minutes and dried in an oven at 60 °C for 6 h to remove the solvent. CZO powder (25 wt%) was mixed with acrylic copolymer emulsion, and the mixture was stirred with the ultrasonication method till a homogeneous solution was achieved. Then, 5, 25, 50, and 100 µm of the solution was poured on a prepared glass substrate and cast coating glass using a four-sided film applicator, which was operated manually. For 50 wt% and 75 wt% of CZO to an acrylic copolymer, they were prepared using the same process as for 25 wt%.

For the composite coating solution with PVP as a dispersant, 0.35 g of PVP was dissolved in 25 mL of ethanol; then, CZO powder was added into the solution, stirred via ultrasonication, and dried in an oven at 60 °C for 6 h to remove the solvent. The weight percentages of CZO powder were varied from 25 wt% to 75 wt% into an acrylic copolymer, and the coating thickness, determined by the aforementioned applicator, was varied from 5 µm to 100 µm, the same as for the method used for the CZO/polymer coating without the PVP.

## 2.4. Characterization

The structure of the CZO powder was characterized by X-ray diffraction (XRD, Malvern PANalytical Aeris, Almelo, The Netherlands) in the 2θ range 20–80° with a 0.02° scan increment. Field-emission scanning electron microscopy (FE-SEM, SU 8000 Hitachi, Tokyo, Japan) was used to study the morphology of the CZO NPs. The optical properties of all powders were investigated using a UV-Vis-NIR spectrophotometer (Agilent Technologies, Santa Cary 5000, Santa Clara, CA, USA) in a wavelength ranging from 200 to 2500 nm. The NIR-shielding property of the coated glass substrate was investigated using a digital thermometer data logger (Testo 175T3, West Chester, IL, USA).

## 2.5. Thermal Insulation Test

The thermal insulation performance of the coated glass was investigated using a white foam box (size 21 cm × 30 cm × 25 cm) to represent a house. The coated glass was placed on the top of the box, and the IR (150 W) light was irradiated onto the glass for 1 h. The temperature on the surface glass (T<sub>1</sub>) and the temperature inside the box (T<sub>2</sub>) were recorded

simultaneously using a thermometer data logger. The insulation test setup was as is shown in Figure 1.

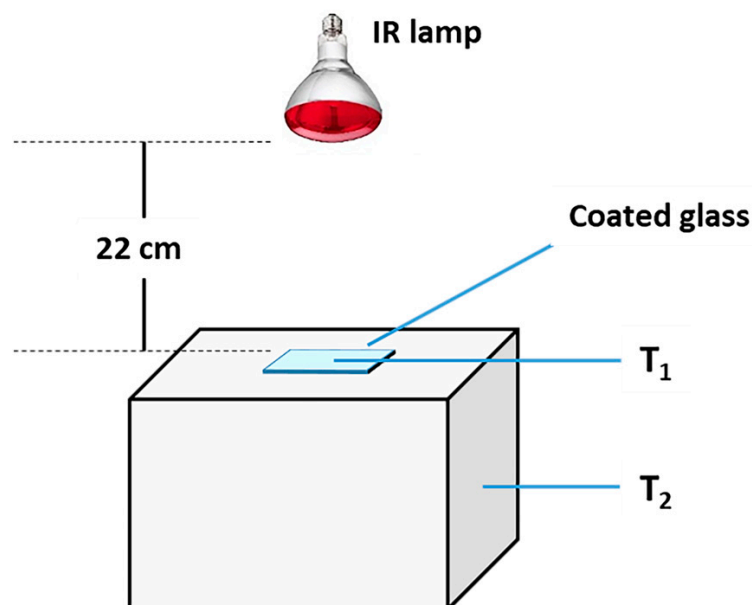


**Figure 1.** House setup for IR thermal insulation testing.

### 3. Results and Discussion

The CZO powder, obtained using molar ratios of the dopant Cu/(Cu + Zn) of 0, 1, 5, and 10 mol%, was synthesized using the sol-gel process after being calcinated at 550 °C for 1 h. The CZO powder/acrylic copolymer was coated on a glass substrate with and without adding polyvinylpyrrolidone (PVP).

#### 3.1. Powder X-ray Diffraction (XRD) Analysis

Figure 2 shows the XRD pattern of CZO in Cu<sup>2+</sup> concentrations of 0, 1, 5, and 10 mol%; 0 mol% Cu was undoped—ZnO acted as a standard material. The analysis of all diffraction peaks was matched with a hexagonal wurtzite ZnO structure (JCPDS File Card No. 36-1451) [25–27]. The observed diffraction peaks at  $2\theta$  were 31.67°, 34.43°, 36.21°, 47.54°, 56.60°, 62.91°, 66.31°, 67.93°, and 69.15°, referring to the (100), (002), (101), (102), (110), (103), (200), (112), and (201) crystal planes, respectively. We found that when there was an increase in the Cu doping sample, the intensity of all diffraction peaks negligibly decreased. These occurrences proved that the Cu<sup>2+</sup> ion had replaced the Zn<sup>2+</sup> ion due to the ionic radius of Cu<sup>2+</sup> (0.73 Å) being very close to that of Zn<sup>2+</sup> (0.74 Å) [28]. However, there were some secondary phases of CuO appearing at 5 and 10 mol% Cu doping. The disadvantage of the secondary phase was that it affected the microstructure and properties. The diffraction peaks of CuO were found at  $2\theta = 35.50^\circ$  and  $38.65^\circ$ , referring to the (311) and (111) planes, because excess Cu<sup>2+</sup> ions may form in the second phase rather than be replaced in the ZnO lattice. This indicated that the limitation of Cu atoms in the ZnO lattice was less than 5 mol%.

In many reported works, the solid solubility limits of Cu in ZnO differ greatly. As reported by Mukhtar et al. [29], the solid solubility of Cu in ZnO can be 11 mol% with the use of a co-precipitation method. Also, by using a co-precipitation method, Muthukumaran et al. [30] claimed that the solid solubility limit was below 6 mol%. The Cu<sup>2+</sup> occupied the Zn<sup>2+</sup> without changing the crystal structure. Moreover, Jongnavakit et al. [31] reported that with the sol-gel process used in this study, Co doping as low as 0.5 mol% was plausible. Overall, the Cu solubility limit in the ZnO lattice depends greatly on the synthesis method.

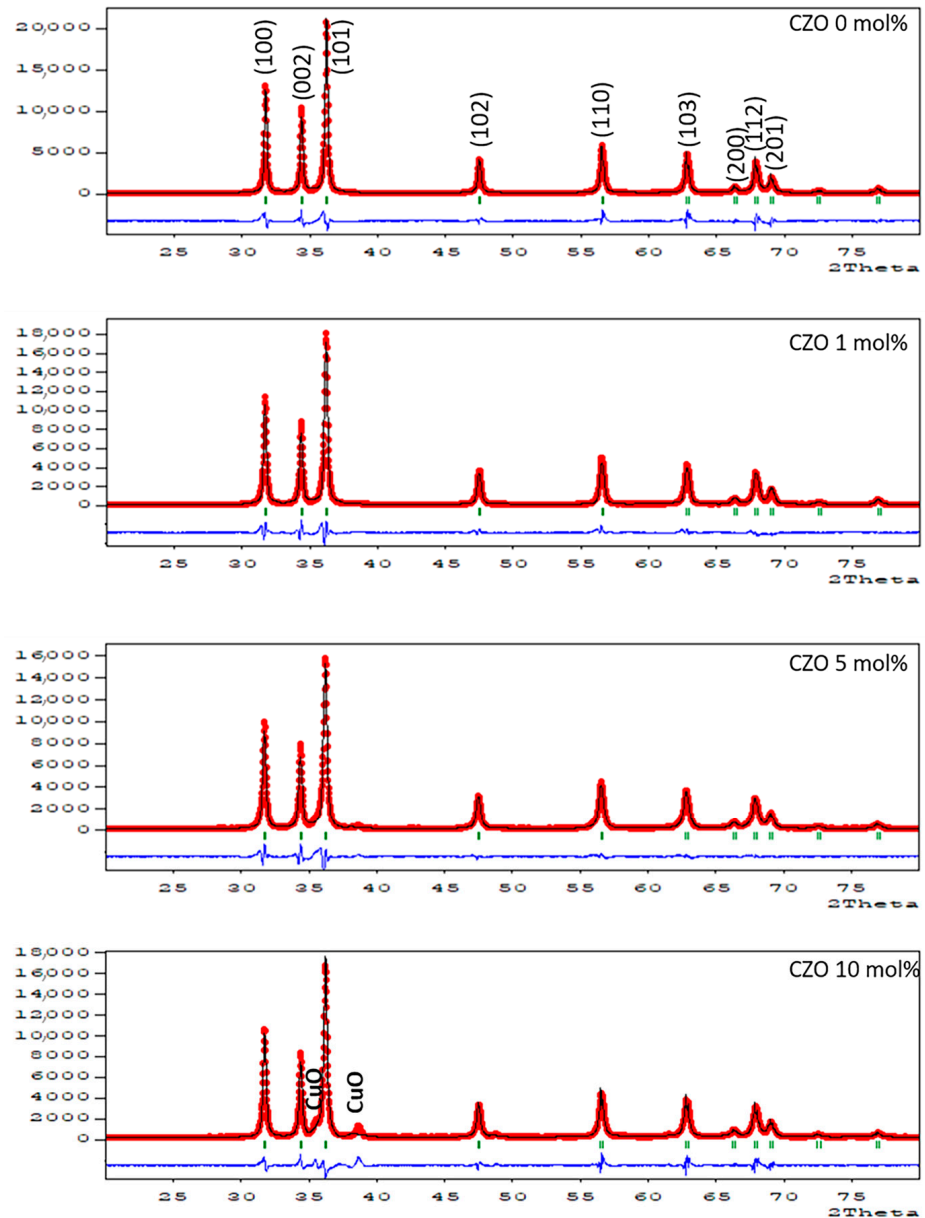


**Figure 2.** Rietveld refinement of X-ray diffraction data of CZO nanopowder at room temperature.

Rietveld refinement of XRD analysis was carried out to determine the structural properties, such as phase formation and crystal structures, of the prepared CZO NPs. The inter-planer spacing, or  $d$ -spacing, was determined by the formula for Bragg's law, which is as follows:

$$d = \frac{n\lambda}{2\sin\theta} \quad (1)$$

where ' $d$ ' is  $d$ -spacing,  $\lambda$  is the X-ray wavelength (Cu K $\alpha$  radiation equals 1.5406 Å), and  $\theta$  is the Bragg diffraction angle. Values related to diffraction peaks, such as  $2\theta$ ,  $(hkl)$ , and inter-planer spacing  $d_{hkl}$ , are summarized in Table 1. From XRD data, the lattice constants ' $a$ ' and ' $c$ ' of the hexagonal ZnO wurtzite structure are found using the following formula:

$$\frac{1}{d^2} = \frac{h^2 + k^2}{a^2} + \frac{l^2}{c^2} \quad (2)$$

**Table 1.** Lattice parameters of hexagonal CZO nanoparticles.

Samples	$2\theta$ (°)	<i>d</i> -Spacing of (101) (Å)	Lattice Parameter ( <i>a</i> ) (Å)	Lattice Parameter ( <i>c</i> ) (Å)
CZO 0 mol%	36.2287	2.4775	3.2508	5.2101
CZO 1 mol%	36.2035	2.4792	3.2519	5.2130
CZO 5 mol%	36.21386	2.4785	3.2517	5.2115
CZO 10 mol%	36.2223	2.4780	3.2509	5.2100

Table 1 compares the lattice parameters between the undoped ZnO and Cu-doped ZnO (CZO) with different dopant concentrations in terms of *d*-spacing and lattice parameter values. It is interesting to note that the *d*-spacing and lattice parameter values CZO were higher than that of undoped ZnO. At 1 mol%, CZO showed the highest values of all parameters, followed by 5 and 10 mol%, while the undoped ZnO showed the lowest values of all parameters. The lattice parameters of undoped—ZnO are close to the parameter of  $a = 3.2500 \text{ \AA}$  and  $c = 5.2070 \text{ \AA}$  from JCPDS data of ZnO. The values of the lattice parameters for the different Cu concentration give slightly higher than undoped—ZnO. The increase in the value of the lattice parameter suggests the possibility of substituting Cu dopants into the Zn sites.

### 3.2. The Morphologies of the CZO Powders

The morphologies of the CZO powders were characterized using FE-SEM with an accelerating voltage of 10 kV. Figure 3 shows FE-SEM micrographs of the CZO powders for Cu doping concentrations of 0, 1, and 10 mol% (there are no data for 5 mol% CZO). All of the micrographs presented grains of particles that were quite similar in size (about 50–100 nm) and morphology. These showed the formation of a quasi-spherical shape and the packing of nanoparticles aggregates. We found also that the size of aggregates was more than 100 nm. The aggregation of particles occurs whenever single nanoparticles cluster together, forming larger objects; it occurs due to the attractive forces between nanoparticles.

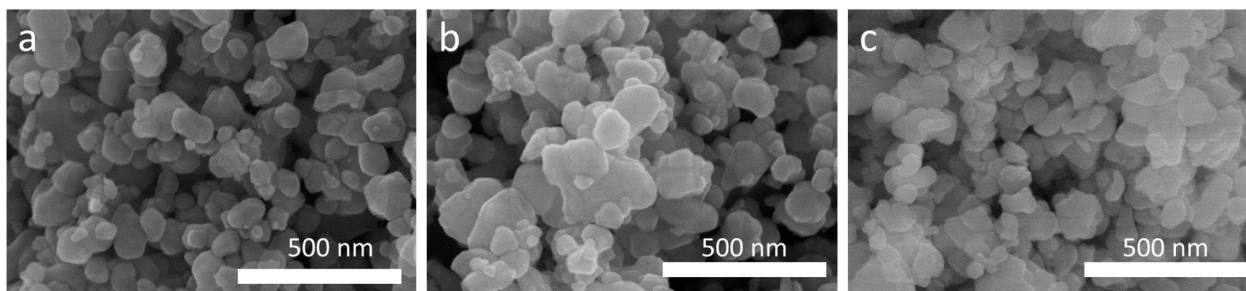


**Figure 3.** FE-SEM micrographs of as-synthesized CZO powders: (a) 0 mol%, (b) 1 mol%, and (c) 10 mol% (100k $\times$  magnification).

### 3.3. The Optical Properties of the CZO Powders

The influence of  $\text{Cu}^{2+}$  content on the optical properties of ZnO powder was investigated based on reflectance spectra determined by using a UV-Vis-NIR spectrophotometer.

Figure 4 shows the reflectance spectra obtained at room temperature for the undoped ZnO (0 mol%) and Cu-doped ZnO (1, 5, and 10 mol%) powders. It was found that CZO 1 mol% represented the highest NIR (in the wavelength of 780–2500 nm) reflectance (up to 80%), followed by CZO 0, 5 and 10 mol%, respectively. CZO 0 mol% showed high NIR reflectance, the same as CZO 1 mol%; however, it showed low visible light (in the wavelength of 400–780 nm) transmission. This means that visible light passed through the window less frequently than for the others. For the Cu-doped ZnO (1, 5, and 10 mol%), it showed a reflectance spectra trend from 1 mol%, followed by 5 and 10 mol%, respectively, with similar reflection characteristics. The CZO powder, at 1, 5, and 10 mol%, presented low

visible light reflectance and, therefore, high visible light transmission, that is, the visible light can pass through the sample, causing transparency to occur. Most of the visible light is transmitted because of the large bandgap of the CZO NPs [32]. The band gap of CZO material is about 3.7 to 3.09 eV, depending on the Cu doping concentration [33]. The visible spectrum is between 3.1 eV and 1.6 eV (wavelength ~400–780 nm). The band gap of CZO material is higher than the maximum energy of visible light; only a small part of the visible light is absorbed, while most of visible light passes through the material. Therefore, the CZO materials appeared more transparent. At 10 mol%, the lowest visible light reflectance was presented, which means that visible light can be transmitted more than in the other samples; however, NIR reflectivity was poor at around 50–60%. While CZO 0 mol% showed high reflectivity in visible NIR regions at about 65–70%. Even though CZO 0 mol% had high NIR reflectivity, meaning that it can reflect more heat in solar light, the drawback was that the visible light could not pass through the sample, or it passed through the sample less than with other samples. This indicates that CZO 1 mol% could be a great sample, with high NIR light reflectivity and good visible light transmission; furthermore, CZO 1 mol% could be used to effectively coat the acrylic copolymer emulsion.

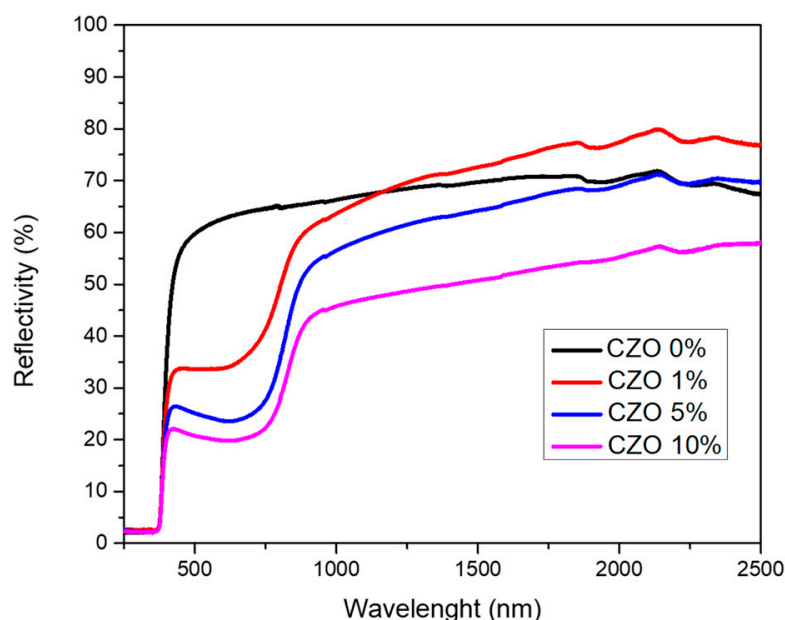


**Figure 4.** UV-Vis-NIR reflectance spectra of CZO powders with different Cu doping contents.

### 3.4. The Optical Properties of the CZO/Acrylic Copolymer Coatings

After that, CZO 1 mol% was chosen to coat the glass substrate as a window whilst we varied the weight of percentage between 25, 50, and 75 wt% CZO powder to an acrylic copolymer and differentiated the thickness of the coating between 5, 25, 50, and 100  $\mu\text{m}$  by using an applicator. We used an acrylic copolymer as the polymer matrix due to its advantages, such as its good hydrophobicity, non-toxicity, and optical transparency. All these coating glasses were light black in color. The samples are shown in Figure 5. The 5  $\mu\text{m}$  thick CZO/acrylic copolymer with 25 wt% CZO showed high transparency to the naked eye, more so than others due to it having the smallest amount of CZO powder, while the 100  $\mu\text{m}$  thick CZO/acrylic copolymer with 75 wt% CZO with the highest amount of CZO powder presented poor transparency. With a high amount of powder, the dispersion of the powder in the polymer was more difficult than with a small amount of powder and indigent dispersibility. However, the coated glass was uniform, and no cracks formed in the samples.

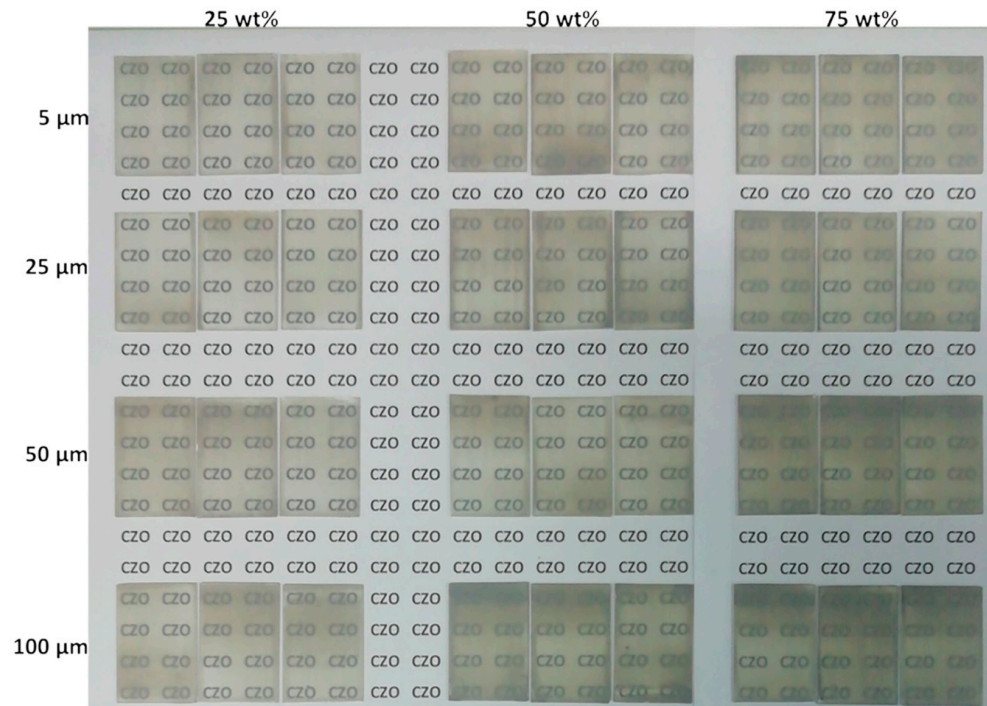


**Figure 5.** CZO nanopowders coated on glass substrates by varied weight percentage of CZO content to acrylic copolymer (25, 50, and 75 wt%) and varying thicknesses (5, 25, 50, and 100 μm).

For comparison, we also measured the transmittance spectrum of the coated glass samples with different Cu (1 mol%) contents (25, 50, and 75 wt%) mixed in acrylic copolymer emulsion and different thicknesses (5, 25, 50, and 100 μm). Obviously, with an increase in CZO content from 25 to 75 wt% and an increase in the thickness of the coating from 5 μm to 100 μm, the transmittance spectrum in the entire UV-vis-NIR region (200–2500 nm) of all samples decreased. This was due to there being more CZO nanoparticles with a light black color, as shown in Figures 6a,b and 7c.

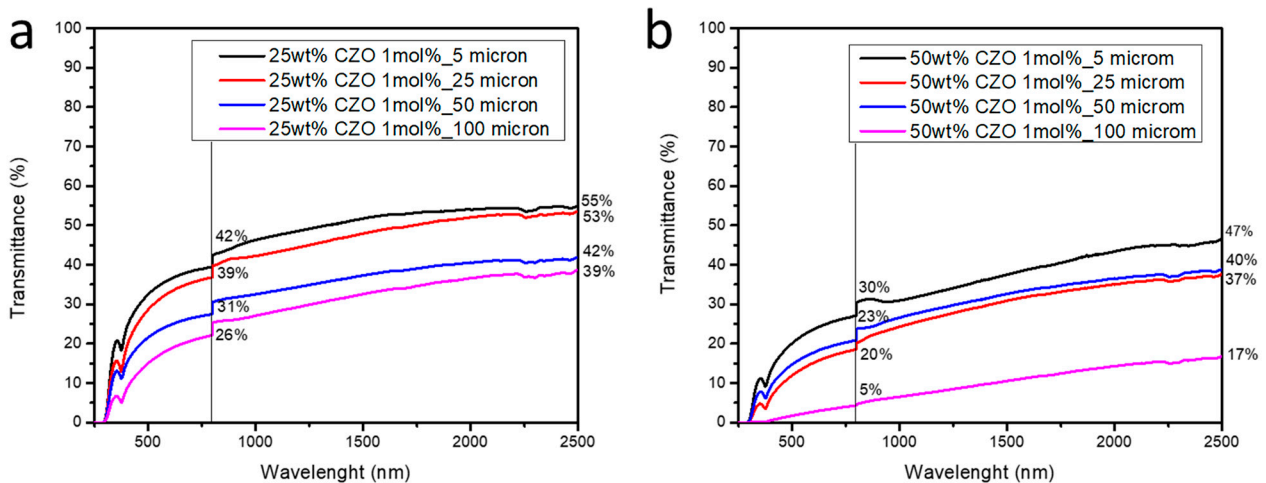


**Figure 6.** Transmittance spectra of CZO/acrylic copolymer-coated glass substrates with different thicknesses (5, 25, 50, and 100 μm): CZO 1 mol% of (a) 25 wt% CZO content and (b) 50 wt% CZO content in acrylic copolymer.

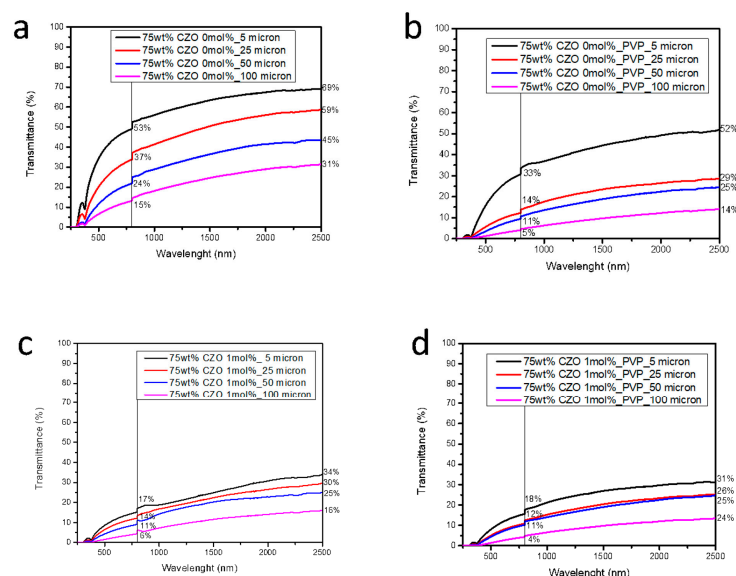


**Figure 7.** Transmittance spectra of CZO/acrylic copolymer-coated glass substrates with different thicknesses (5, 25, 50, and 100  $\mu\text{m}$ ) (75 wt% CZO/acrylic copolymer): (a) CZO 0 mol% without PVP, (b) CZO 0 mol% with PVP, (c) CZO 1 mol% without PVP, and (d) CZO 1 mol% with PVP.

For example, the 75 wt% CZO (1 mol%)/acrylic copolymer with a coating thickness of 100  $\mu\text{m}$  exhibited very low transmittance in all UV-vis-NIR ranges, and at 2500 nm (maximum wavelength ( $\lambda_{\text{max}}$ ) in NIR region), it presented only 16% transmittance (T) compared to the thinnest coating (5  $\mu\text{m}$ ), which had about 34% transmittance. These results were also observed with 50 wt% (100  $\mu\text{m}$  thick;  $T_{2500\text{nm}} = 17\%$  and 5  $\mu\text{m}$  thick;  $T_{2500\text{nm}} = 47\%$ ) and 25 wt% CZO content (100  $\mu\text{m}$  thick;  $T_{2500\text{nm}} = 39\%$  and 5  $\mu\text{m}$  thick;  $T_{2500\text{nm}} = 55\%$ ). Due to an increase in the CZO content with greater thickness, the amount of CZO powder on the coating increased, and the light transmittance in all ranges was poor. However, the 100  $\mu\text{m}$  thick 75 wt% CZO content polymer-coated glass substrate was transparent, though there was a lack of smoothness. Therefore, we added polyvinylpyrrolidone (PVP) to act as a dispersant to disperse CZO powder into the acrylic copolymer before coating the glass. We used PVP due to the fact that it is hydrophilic and can be easily dispersed in ethanol, which was a solvent in the solution, and ethanol was also completely evaporated.

Figure 8 shows the transmittance spectra of glass and acrylic copolymer-coated glass substrates which acted as standard references. These two materials showed high transmittance mostly in the UV to NIR radiation ranges. The transmittance spectra of both showed a similar trend due to our %T mode measurements involving the use of glass, which acted as a solid material so that the light source could pass through the sample. The optical property of acrylic copolymer is transparent, and most acrylic polymers will allow light of wavelengths greater than  $\sim 290$  nm to pass through the material. Therefore, the %T of the acrylic copolymer-coated glass presented the same transmittance spectra as the glass substrate.

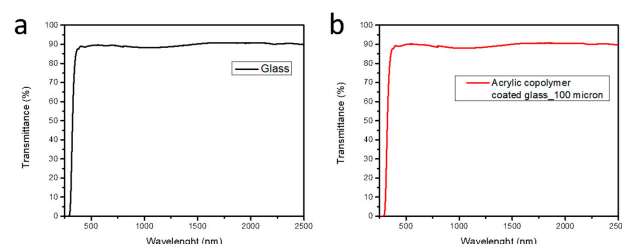


**Figure 8.** The transmittance spectra of (a) the glass substrate and (b) the acrylic copolymer-coated glass substrate (100  $\mu\text{m}$  thick).

### 3.5. The Optical Properties of the CZO/Acrylic Copolymer Coatings with and without PVP

Figure 9 shows 75 wt% CZO/acrylic copolymer coatings, which were placed on the glass substrates, with 0 mol% and 1 mol% Cu doping concentrations and varying thicknesses (5, 25, 50, and 100  $\mu\text{m}$ ). The left side of the figure shows those without the PVP dispersant, while the right side of the figure shows those with the PVP dispersant. The dispersion containing CZO nanoparticles exhibited a strong white color for CZO 0 mol% (Figure 9a), a light black color for CZO 1 mol% (Figure 9b), and had high stability, even remaining unchanged for several weeks. Obviously, when the CZO/acrylic copolymer coating with PVP was added, the smoothness and dispersion state of the glass coating were better than that of the coating without PVP, while the glass coating without PVP had agglomerated together, leading to the poor transparency of the coating, thus indicating that PVP acted as a dispersant and played a crucial role in the stabilization of CZO nanoparticles. All these coating samples were also measured in terms of their transmittance, as shown in Figure 7. The transmittance spectrum of the 75 wt% CZO/acrylic copolymer in CZO 0 mol% and 1 mol% with PVP (Figure 7b,d), in all wavelengths, presented lower values than that of the coating without PVP (Figure 7a,c) due to the fact that adding more material, namely PVP, led to a greater amount of substances in aqueous solution, and the optical indistinctness was also increased. In addition, CZO nanopowder can transmit visible light and also shield NIR light more effectively than the bare glass substrate and 100  $\mu\text{m}$  thick acrylic copolymer, which transmitted light in almost all wavelengths, from UV to NIR.

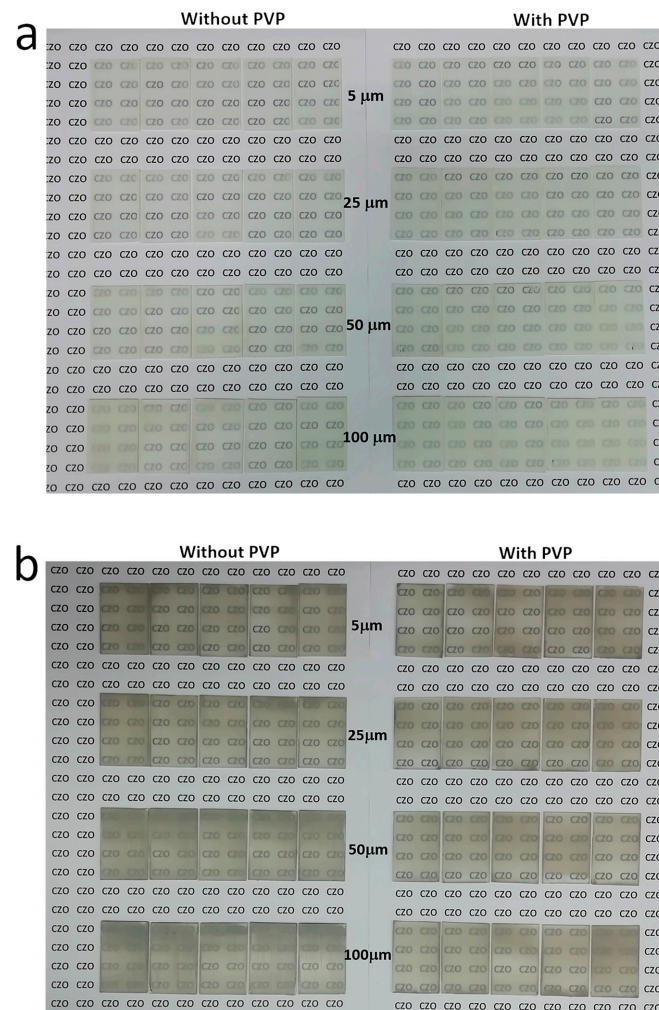


**Figure 9.** CZO/acrylic copolymer coatings applied to glass substrates with 75 wt% CZO content in acrylic copolymer with different thicknesses (5, 25, 50, and 100  $\mu\text{m}$ ): (a) CZO 0 mol% without/with PVP and (b) CZO 1 mol% without/with PVP.

### 3.6. The Thermal Shielding Effects

The thermal shielding performance of the CZO coating samples was tested using the aforementioned thermal insulation experimental setup. Figure 10 plots the temperature on the glass surface ( $T_1$ ) and the interior air temperature of the box ( $T_2$ ) upon irradiation time in the average (last 20 m) time. It was found that when the glass surface was irradiated for 1 h, the temperature of the CZO coating surface ( $T_1$ ) tended to increase with an increase in weight percentages from 25 to 75 wt% and an increase in thickness from 5 to 100  $\mu\text{m}$  due to the amount of powder in the coating glass and the heat (NIR light) reflectance of the CZO nanopowder, as revealed with the use of the UV-vis-NIR spectrophotometer (Figure 4). The lowest  $T_1$  with increasing weight percentage and film thickness belonged to the glass substance (70.6  $^{\circ}\text{C}$ ), followed by the acrylic copolymer coating (70.7  $^{\circ}\text{C}$ ) and CZO-coated glass. The 75 wt% CZO/acrylic copolymer showed the highest temperature (from 73.0 to 75.6  $^{\circ}\text{C}$ ), and the maximum temperature was achieved at 100  $\mu\text{m}$  thickness. Regarding the temperature inside the box ( $T_2$ ) after IR light exposure, it also tended to increase in the same manner as the  $T_1$ . The  $T_2$  of the 25 wt% and 50 wt% CZO/acrylic copolymers showed similar values with the same coating thicknesses (5, 25, 50, and 100  $\mu\text{m}$ ) in the range of 53.2–54.0  $^{\circ}\text{C}$ , as shown in Figure 10b. And the 100  $\mu\text{m}$  thick 75 wt% CZO/acrylic copolymer coating showed the highest  $T_2$  (around 54.0  $^{\circ}\text{C}$ ). In addition, at 25 wt% (black line) and 50 wt% (red line) and varying the film thickness from 5 to 100  $\mu\text{m}$ , the same trend in  $T_2$  was found, as shown in Figure 10b. However, the 5  $\mu\text{m}$  thick 75 wt% CZO coating presented the lowest  $T_2$ . This result means that this coating could be great for window coating applications because it could help keep interior air temperatures low, keeping indoor areas cooler and also more comfortable for those living in buildings and when using automobiles. Thus, we could use this material as a thermal insulation coating.

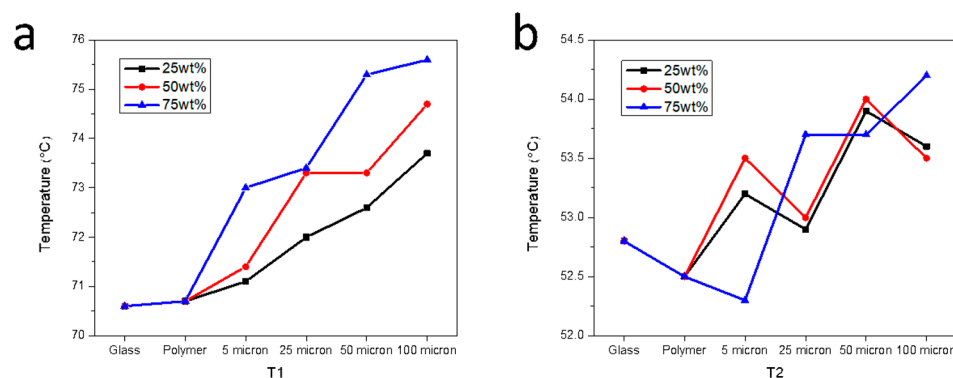


**Figure 10.** Temperature of the coated glass substrates after IR lamp irradiation for 1 h: (a) temperature on glass surface ( $T_1$ ) and (b) temperature inside the foam box ( $T_2$ ) of 25, 50, and 75 wt% CZO (1 mol%)/acrylic copolymers without PVP.

While 75 wt% CZO/polymer coatings with different thicknesses and without and with PVP were also tested in terms of thermal insulation performance, it can be seen that the coating with PVP presented lower  $T_1$  than that of the coating without PVP (about 2.2–4.6  $^{\circ}\text{C}$ ), as shown in Figure 11a, due to the good dispersion of CZO powder on the coating surface (Figure 9b). The advantage of this result is that the surface of this coating was not too high when compared with the CZO coating without PVP. The  $T_1$  of the 75 wt%/acrylic copolymer coating without PVP was 73.0, 73.4, 75.3, and 75.6  $^{\circ}\text{C}$  at 5, 25, 50, and 100  $\mu\text{m}$  thickness, respectively. The 75 wt% CZO/acrylic copolymer coating with PVP showed the lowest  $T_1$  at 70.7  $^{\circ}\text{C}$  (50  $\mu\text{m}$  thick) and the highest  $T_1$  at 72.1  $^{\circ}\text{C}$  (100  $\mu\text{m}$  thick). In addition, the  $T_2$  of those samples (without/with PVP) showed similar values at temperatures between 52.3 and 54.2  $^{\circ}\text{C}$  (Figure 11b). The difference in temperature between the 75 wt% CZO/acrylic copolymer without/with PVP was about 0.4–0.6  $^{\circ}\text{C}$ . It should be noted that the temperature elevation was inevitable because of the CZO powder with its own NIR (which acted as heat) reflectance. However, the inner and outer temperature of

coating glass can be controlled by adjusting the amount of CZO powder, the thickness, the smoothness of the coating, and the combination of the composite particles.

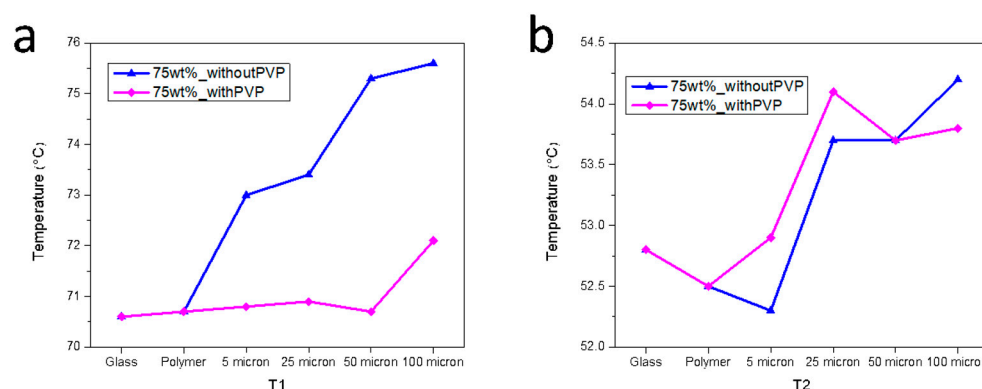


**Figure 11.** Temperature of the coated glass substrates after IR lamp irradiation for 1 h: (a) temperature on glass surface (T<sub>1</sub>) and (b) temperature inside the foam box (T<sub>2</sub>) of 75 wt% CZO (1 mol%)/acrylic copolymers without/with PVP.

#### 4. Conclusions

In summary, CZO NPs were synthesized by the sol–gel method. All the CZO particles had a size of either 0, 1, 5, or 10 mol%, were in the same thickness range of about 50–100 nm, and had a quasi-spherical morphology. At 1 mol%, the CZO powder exhibited the highest NIR reflectance (up to 80%), with great visible light transmission. The CZO 1 mol% nanopowder was mixed in an acrylic copolymer emulsion. When there was an increase in the weight percentages of the CZO powder from 25 to 75 wt% and in the coating thickness from 5 to 100  $\mu\text{m}$ , the reflectance in all UV-vis-NIR radiation ranges (wavelengths 250–2500 nm) decreased due to the increase in the amount of CZO particles with a light black color. Adding PVP in CZO/acrylic copolymers helps to disperse the CZO powder in the polymer and leads to a smooth coating surface with a uniform distribution of particles. The temperature on the glass surface (T<sub>1</sub>) of the 75 wt% CZO (1 mol% Cu-doped) coating/acrylic copolymer with PVP with varying thickness was lower than the coating without PVP, which means that it can reduce the risk of heat exposure after being coated on glass surfaces.

**Author Contributions:** Methodology, P.P., S.K. and D.T.; formal analysis, P.P. and D.T.; investigation, P.P. and S.K.; data curation, P.P.; writing—original draft, P.P.; writing—review and editing, P.P., S.Y. and D.T.; validation, S.K.; conceptualization, S.Y., W.T., N.S., J.J. and D.T.; resources, S.Y., W.T., N.S. and J.J.; supervision, S.Y., W.T., N.S., J.J. and D.T.; project administration, D.T.; funding acquisition, D.T. All authors have read and agreed to the published version of the manuscript.

**Funding:** This research was funded by the Thailand Research Fund and Faculty of Science, Mahidol university (grant no. IRG5980007) and NSTDA-EGAT joint program (grant no. FDA-CO-2561-7467-TH).

**Institutional Review Board Statement:** Not applicable.

**Informed Consent Statement:** Not applicable.

**Data Availability Statement:** Data are contained within the article.

**Acknowledgments:** The authors would like to thank the Faculty of Graduate studies, Mahidol University, Institute for Innovative Learning, Mahidol University, the Center of Nanoimaging, Mahidol University, and the Science Achievement Scholarship of Thailand (SAST), for financial support.

**Conflicts of Interest:** Authors Noppakun Sanpo, Jaturong Jitputti were employed by the company SCG Chemical Co., Ltd. The remaining authors declare that the research was conducted in the absence of any commercial or financial relationships that could be construed as a potential conflict of interest.

## References

1. Jiang, L.; Li, J.; Huang, K.; Li, S.; Wang, Q.; Sun, Z.; Mei, T.; Wang, J.; Zhang, L.; Wang, N.; et al. Low-temperature and solution-processable zinc oxide transistors for transparent electronics. *ACS Omega* **2017**, *2*, 8990–8996. [[CrossRef](#)] [[PubMed](#)]
2. Tuzemen, S.; Gur, E. Principal issues in producing new ultraviolet light emitters based on transparent. *Nanomaterials* **2020**, *10*, 1661.
3. Izaki, M.; Watase, S.; Takahashi, H. Low-Temperature Electrodeposition of Room-Temperature Ultraviolet-Light-Emitting Zinc Oxide. *Adv. Mater.* **2003**, *15*, 2000. [[CrossRef](#)]
4. Du, J.P.; Zhao, R.H.; Chen, S.; Wang, H.Y.; Li, J.P.; Zhu, Z.P. Self-Assembly of Gridlike Zinc Oxide Lamellae for Chemical-Sensing Applications. *ACS Appl. Mater. Interfaces* **2015**, *7*, 5870–5878. [[CrossRef](#)] [[PubMed](#)]
5. Israr-Qadir, M.; Jamil-Rana, S.; Nur, O.; Willander, M. Zinc oxide-based self-powered potentiometric chemical sensors for biomolecules and metal ions. *Sensors* **2017**, *17*, 1645. [[CrossRef](#)] [[PubMed](#)]
6. Wibowo, A.; Marsudi, M.A.; Amal, M.I.; Ananda, M.B.; Stephanie, R.; Ardy, H.; Diguna, L.J. ZnO nanostructured materials for emerging solar cell applications. *RSC Adv.* **2020**, *10*, 42838–42859. [[CrossRef](#)] [[PubMed](#)]
7. Ning, X.; Hao, A.; Cao, Y.; Hu, J.; Xie, J.; Jia, D. Effective promoting piezocatalytic property of zinc oxide for degradation of organic pollutants and insight into piezocatalytic mechanism. *J. Colloid Interface Sci.* **2020**, *577*, 290–299. [[CrossRef](#)] [[PubMed](#)]
8. Noman, M.T.; Petru, M. Functional properties of sonochemically synthesized zinc oxide nanoparticles and cotton composites. *Nanomaterials* **2020**, *10*, 1661. [[CrossRef](#)] [[PubMed](#)]
9. Taie, M.; Fadaei, A.; Sadeghi, M.; Hemati, S.; Mardani, G. Comparison of the Efficiency of Ultraviolet/Zinc Oxide (UV/ZnO) and Ozone/Zinc Oxide (O<sub>3</sub>/ZnO) Techniques as Advanced Oxidation Processes in the Removal of Trimethoprim from Aqueous Solutions. *Int. J. Chem. Eng.* **2021**, *2021*, 9640918. [[CrossRef](#)]
10. Embden, J.; Gross, S.; Kittilstved, K.R.; Gaspera, E.D. Colloidal Approaches to Zinc Oxide Nanocrystals. *Chem. Rev.* **2022**, *123*, 271–326. [[CrossRef](#)] [[PubMed](#)]
11. Tofa, T.S.; Kunjali, K.L.; Paul, S.; Dutta, J. Visible light photocatalytic degradation of microplastic residues with zinc oxide nanorods. *Environ. Chem. Lett.* **2019**, *17*, 1341–1346. [[CrossRef](#)]
12. Krishna Murthy, T.P.; Gowrishankar, B.S.; Krishna, R.H.; Chandrababha, M.N.; Sreenivasa; Rao, R. Influence of Fuel Nature on Dye Adsorption Efficiency of Solution Combustion Derived Zinc Oxide Nanoparticles: A Comparative Study. *Mater. Res. Express* **2019**, *6*, 055512. [[CrossRef](#)]
13. Orante-Barrón, V.R.; Escobar-Ochoa, F.M.; Cruz-Vázquez, C.; Bernal, R. Thermoluminescence of Novel Zinc Oxide Nanophosphors Obtained by Glycine-Based Solution Combustion Synthesis. *J. Nanomater.* **2015**, *2015*, 273571. [[CrossRef](#)]
14. Saravanakumar, K.; Ravichandran, K. Simultaneous doping of aluminum and fluorine on zinc oxide nanopowder using a low-cost soft chemical route. *J. Mater. Sci. Mater. Electron.* **2012**, *23*, 1462–1469. [[CrossRef](#)]
15. Chen, X.L.; Geng, X.H.; Xue, J.M.; Zhang, D.K.; Hou, G.F.; Zhao, Y. Temperature-dependent growth of zinc oxide thin films grown by metal organic chemical vapor deposition. *J. Cryst. Growth* **2006**, *296*, 43–50. [[CrossRef](#)]
16. Tan, S.T.; Sun, X.W.; Zhang, X.H.; Chen, B.J.; Chua, S.J.; Yong, A.; Dong, Z.L.; Hu, X. Zinc oxide quantum dots embedded films by metal organic chemical vapor deposition. *J. Cryst. Growth* **2006**, *290*, 518–522. [[CrossRef](#)]
17. Debanath, M.K.; Karmakar, S. Study of blueshift of optical band gap in zinc oxide (ZnO) nanoparticles prepared by low-temperature wet chemical method. *Mater. Lett.* **2013**, *111*, 116–119. [[CrossRef](#)]
18. Strachowski, T.; Grzanka, E.; Lojkowski, W.; Presz, A.; Godlewski, M.; Yatsunenکو, S.; Matysiak, H.; Piticescu, R.R.; Monty, C.J. Morphology and luminescence properties of zinc oxide nanopowders doped with aluminum ions obtained by hydrothermal and vapor condensation methods. *J. Appl. Phys.* **2007**, *102*, 073513. [[CrossRef](#)]
19. Thambidurai, S.; Gowthaman, P.; Venkatachalam, M.; Suresh, S. Natural sunlight assisted photocatalytic degradation of methylene blue by spherical zinc oxide nanoparticles prepared by facile chemical co-precipitation method. *Optik* **2020**, *207*, 163865. [[CrossRef](#)]
20. Kumar, V.R.; Wariar, P.R.S.; Prasad, V.S.; Koshy, J. A novel approach for the synthesis of nanocrystalline zinc oxide powders by room temperature co-precipitation method. *Mater. Lett.* **2011**, *65*, 2059–2061. [[CrossRef](#)]
21. Natsume, Y.; Sakata, H. Zinc oxide films prepared by sol-gel spin-coating. *Thin Solid Film.* **2000**, *372*, 30–36. [[CrossRef](#)]
22. Alwan, R.M.; Kadhim, Q.A.; Sahan, K.M.; Ali, R.A.; Mahdi, R.J.; Kassim, N.A.; Jassim, A.N. Synthesis of zinc oxide nanoparticles via sol-gel route and their characterization. *Nanosci. Nanotechnol.* **2015**, *5*, 1–6.
23. Peng, L.H.; Xu, Z.Q.; Chao, L.M.; Zheng, D.P.; Yang, H.B.; Sun, C.W.; Cui, H.Z. New energy-saving building developed by using polyethylene glycol/halloysite nanotube energy-storage blanket and heat-insulating glass with Na<sub>2</sub>WO<sub>3</sub>@SiO<sub>2</sub> nano-coating. *Sol. Energy Mater. Sol. Cells* **2023**, *250*, 112074. [[CrossRef](#)]
24. Safo, I.A.; Werheid, M.; Dosche, C.; Oezaslan, M. The role of polyvinylpyrrolidone (PVP) as a capping and structure-directing agent in the formation of Pt nanocubes. *Nanoscale Adv.* **2019**, *1*, 3095–3106. [[CrossRef](#)] [[PubMed](#)]
25. Alibe, I.M.; Matori, K.A.; Sidek, H.A.A.; Yaakob, Y.; Rashid, U.; Alibe, A.M.; Zaid, M.H.M.; Nasir, S.; Nasir, M.M. Effects of polyvinylpyrrolidone on structural and optical properties of willemite semiconductor nanoparticles by polymer thermal treatment method. *J. Therm. Anal. Calorimet.* **2019**, *136*, 2249–2268. [[CrossRef](#)]
26. Yedurkar, S.; Maurya, C.; Mahanwar, P. Biosynthesis of Zinc Oxide Nanoparticles Using *IxoraCoccinea* Leaf Extract—A Green Approach. *Open J. Synth. Theory Appl.* **2016**, *5*, 1–14.
27. Kandulna, R.; Choudhary, R.B. Concentration-dependent behaviors of ZnO-reinforced PVA–ZnO nanocomposites as electron transport materials for OLED application. *Polym. Bull.* **2018**, *75*, 3089–3107. [[CrossRef](#)]

28. Singhal, S.; Kaur, J.; Namgyal, T.; Sharma, R. Cu-doped ZnO nanoparticles: Synthesis, structural and electrical properties. *Phys. B Condens. Matter* **2012**, *407*, 1223–1226. [[CrossRef](#)]
29. Mukhtar, M.; Munisa, L.; Saleh, R. Co-Precipitation Synthesis and Characterization of Nanocrystalline Zinc Oxide Particles Doped with Cu<sup>2+</sup> Ions. *Mater. Sci. Appl.* **2012**, *3*, 543–551.
30. Muthukumaran, S.; Gopalakrishnan, R. Structural, FTIR and photoluminescence studies of Cu doped ZnO nanopowders by co-precipitation method. *Opt. Mater.* **2012**, *34*, 1946. [[CrossRef](#)]
31. Jongnavakit, P.; Amornpitoksuk, P.; Suwanboon, S.; Ndiege, N. Preparation and photocatalytic activity of Cu-doped ZnO thin films prepared by the sol–gel method. *Appl. Surf. Sci.* **2012**, *258*, 8192–8198. [[CrossRef](#)]
32. Su, K.; Mao, Z.; Yang, Z.; Zhang, J. Preparation and characterization of PVC/CsxWO<sub>3</sub> composite film with excellent near-infrared light shielding and high visible light transmission. *J. Vinyl Addit. Technol.* **2021**, *27*, 356–366. [[CrossRef](#)]
33. Dejam, L.; Kulesza, S.; Sabbaghzadeh, J.; Ghaderi, A.; Solaymani, S.; Țălu, Ș.; Bramowicz, M.; Amouamouha, M.; Shayegan, A.h.S.; Sari, A.h. ZnO, Cu-doped ZnO, Al-doped ZnO and Cu-Al doped ZnO thin films: Advanced micro-morphology, crystalline structures and optical properties. *Results Phys.* **2023**, *44*, 106209. [[CrossRef](#)]

**Disclaimer/Publisher’s Note:** The statements, opinions and data contained in all publications are solely those of the individual author(s) and contributor(s) and not of MDPI and/or the editor(s). MDPI and/or the editor(s) disclaim responsibility for any injury to people or property resulting from any ideas, methods, instructions or products referred to in the content.